Correcting GNSS NLOS by 3D LiDAR and Building Height

Weisong Wen
Department of Mechanical Engineering, The Hong Kong Polytechnic University
Guohao Zhang, Li-Ta Hsu*
Interdisciplinary Division of Aeronautical and Aviation Engineering, The Hong Kong Polytechnic University

BIOGRAPHY (IES)

Weisong WEN is a PhD. candidate at the Department of Mechanical Engineering, The Hong Kong Polytechnic University, Hong Kong. His research interests include GNSS/INS/LiDAR/HD Map-based localization for autonomous vehicles and deep learning-based object detection.

ABSTRACT

Occurrence of autonomous driving introduces high requirement in GNSS positioning performance. GNSS is currently the only source providing absolute positioning information. It is indispensable for initial position estimation for the high definition map-based localization solution in autonomous driving. Satisfactory positioning accuracy can be obtained in open space or sub-urban areas. However, its performance is heavily challenged in super-urbanized scenarios with the positioning error going up to even 100 meters, due to the well-known NLOS receptions which dominates the GNSS positioning errors. The recent state-of-art range-based 3D map aided GNSS (3DMA GNSS) can mitigate most of the NLOS receptions. However, ray-tracing simulation is time-consuming. Therefore, we present a novel method to detect the NLOS caused by surrounding buildings and correct the pseudorange measurements using 3D point clouds and building height without ray-tracing simulation. To estimate the geometry and pose of the building relative to GNSS receiver, a surface segmentation method is employed to detect the surrounding building walls. NLOS errors are estimated by integrating the geometry, pose relative to the GNSS receiver and satellites information. Finally, position estimation of GNSS receiver is implemented by weighted least square (WLS) based on the corrected and healthy pseudorange measurements. Dynamic experiment is conducted to evaluate the errors caused by the NLOS receptions and to verify the effectiveness of the proposed method in a deep urbanized area, Hong Kong.

1. INTRODUCTION

To achieve fully autonomous driving in all scenarios, centimeter-level absolute positioning is required. Light detection and ranging (LiDAR), camera and inertial navigation system (INS) are commonly used in positioning and only relative positioning information is obtained. Thus, these sensors are usually integrated with Global Navigation Satellites System (GNSS) information [1-4], as GNSS is currently the only source that can provide the absolute positioning relative to the earth. The GNSS/INS/LIDAR/HD map-based solution can provide satisfactory localization information in sub-urban [5, 6] area with the condition that enough direct signals transmitted from multi-constellation satellite navigation systems (GPS, BeiDou, GLONASS, Galileo and QZSS), so called line-of-sight (LOS) [7]. However, the signals from satellites can be reflected, blocked and diffracted by surrounding buildings in urbanized area, such as Tokyo and Hong Kong, introducing the well-known NLOS receptions which dominant the GNSS positioning errors [8]. As a result, the positioning error can go up to even 100 meters [9, 10]. More importantly, the exact error covariance model [11] of GNSS positioning in urbanized area is also unknown which is significant for sensor fusion framework.

Numerous methods are studied to mitigate the localization errors caused by NLOS receptions. NLOS receptions contain only the indirect signals. As performance of GNSS positioning relies heavily on the environment features, such as the buildings, utilizing the 3D building model to detect the NLOS is straightforward. NLOS can be detected with the aid of building model and then be excluded from GNSS positioning [12, 13]. However, the NLOS exclusion will introduce a distortion of satellites distribution, which will enlarge the lateral positioning error especially in super urbanized area. To effectively detect the NLOS receptions and correct the corresponding pseudorange measurements, range-based 3DMA GNSS [14-17] is proposed to simulate the GNSS signals transmission routes using the well-understood ray-tracing [18] method. The ranging-based 3DMA GNSS [14-16] can detect and correct NLOS receptions using ray-tracing simulation. However, performance of this method is subjected to the accuracy and availability of 3D city maps and rely heavily on the time-consuming ray-tracing process, which are now the

main difficulties for the implementation of 3DMA GNSS. Increasing field of view (FOV) for LiDAR sensor makes it possible to partially reconstruct the environment or sense the environment in real time. Constructed map of environment using 3D LiDAR is employed to detect the visibility of satellites [11]. To better model the reliability of GNSS solution, both horizontal dilution of precision and SNR are integrated to calculate error covariance. Deep coupling of GNSS and LiDAR is proposed [19]. A fully software-based multipath corrector is developed in GNSS receiver using the Amplitude Delay Lock Loop (CADLL) architecture [20]. The multipath detection result from CADLL is compared with the parameters of environments features identified by the LiDAR sensor, such as the surface features. Thus, this method relies heavily on the environment features. To detect the visibilities of satellites, omnidirectional camera [21, 22] is used to detect the skylines of buildings in urbanized area. NLOS receptions can be detected with the detected skylines and some improvements are obtained. However, this method can suffer from the strong light or night scenarios, as computer vision technique is employed to detect the skylines. Moreover, this method excludes the NLOS satellites which can cause lack of satellites numbers for GNSS positioning calculation or introduce big distortion of satellites distribution in super-urbanized area. The NLOS correction is the more potential way to improve the GNSS positioning performance in which both NLOS and LOS measurements are used.

Generally, 3DMA GNSS can obtain most effective improvements in mitigating the NLOS errors. The main problem for its implementation is the high computational load introduced by ray-tracing process. GNSS positioning errors caused by NLOS receptions are clearly analyzed [9] and signal transmission delay caused by NLOS is also calculated. However, the distance from the receiver to the buildings is manually estimated from Google Maps afterwards

In this paper, we propose to detect and correct the NLOS receptions caused by surrounding buildings in urbanized scenarios using real-time 3D point cloud generated by LiDAR and building height without ray-tracing process. Moreover, only rough building height information are needed. The 3D LiDAR is widely used in autonomous driving vehicles [23, 24]. Thus, we innovatively employ the LiDAR to obtain the point clouds corresponding to the surrounding buildings to facilitate GNSS positioning. Dimension and pose of the building wall relative to GNSS receiver is calculated using the point clouds-based segmentation. Distance between GNSS receiver and buildings can be obtained subsequently. Due to the limited field of view (FOV), tall building cannot be fully scanned. Thus, height of the detected building wall is extended to the exact height provided by a building height list obtained from Google maps. Based on the detected building wall boundaries, NLOS detection and correction can be implemented with a NLOS error model. Finally, GNSS positioning result is calculated based on the corrected pseudorange measurements and healthy pseudorange measurements.

The remainder of this paper is structured as follows. An overview of the proposed method is given in Section 2. Section 3 discusses building surface detection method process. Coordinate transformation from LiDAR coordinate system to skyplot coordinate system is also presented in this section. In Section 4, NLOS detection criterion is proposed and NLOS correction model is introduced. Then, WLS-based GNSS positioning is introduced. In Section 5, we evaluate the effectiveness of the proposed method by means of dynamic experiments. Finally, conclusions and future work are withdrawn in Section 6

2. OVERVIEW OF THE PROPOSED METHOD

In this study, we focus on the NLOS receptions caused by surrounding buildings. Fig. 1 presents direct propagation routes and potential NLOS receptions of GNSS signal. The buildings (height is **H**) can block signal transmitted from the satellite. Meanwhile, this GNSS signal is reflected by nearby building and finally received by GNSS receiver equipped on top of the autonomous vehicle, which results in NLOS receptions. Such kind of scenario is quite common in super-urbanized area in Hong Kong. In this case, number of satellites visible is related to the height of buildings and the distance from the receiver to the building (**α** in Fig. 1).

As an irreplaceable sensor for positioning and perception of autonomous driving, 3D LiDAR is equipped on the top as shown in Fig. 1. In this study, LiDAR is employed to detect the surrounding building surfaces and obtain the distance from GNSS receiver to building surface. Then, NLOS detection and correction are implemented consequently based on detected building surface parameters which are projected into a skyplot with satellites, and the distance from GNSS receiver to buildings. Finally, GNSS positioning is proceeded using both the corrected and healthy pseudorange measurements. Fig. 2 shows the flowchart of the proposed method. The proposed method can be executed as follows:

Step I: Point clouds segmentation method is employed to detect the building surface and corresponding geometry dimensions and pose relative to GNSS receiver is calculated. Distance between GNSS receiver and buildings can be obtained subsequently. Moreover, building height from Google Maps is employed to extend the detected building surface to the exact height.
Step II: Satellites and building boundaries are projected into a skyplot based on their azimuth and elevation angles relative to the GNSS receiver.
Step III: Considering satellites elevation angle, azimuth angle, SNR and building boundary information (elevation and azimuth angles in skyplot), satellites blocked by building are detected. Then NLOS correction is implemented with a NLOS error model.
Step IV: Implementing GNSS positioning using the corrected pseudorange measurements and healthy pseudorange measurements.
The details of the algorithms are introduced in the following sections.
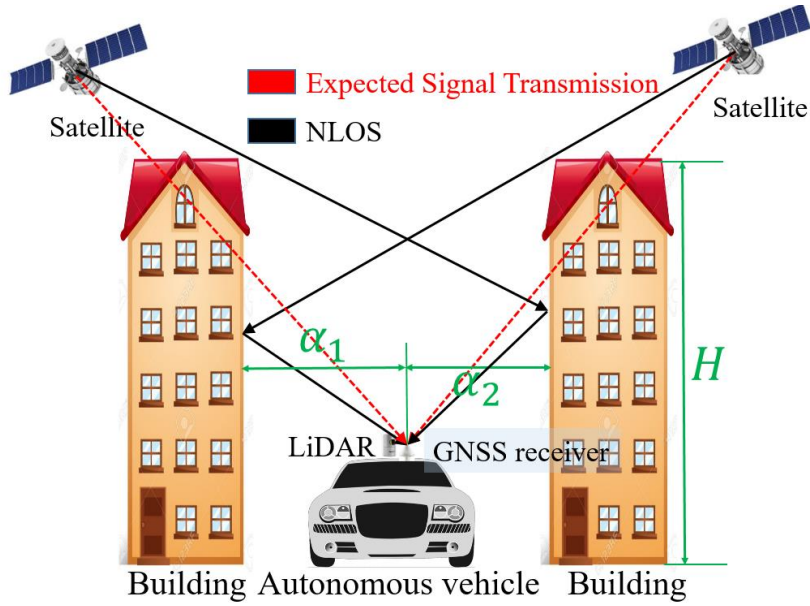
Fig.1 Illustration of NLOS receptions caused by surrounding buildings.
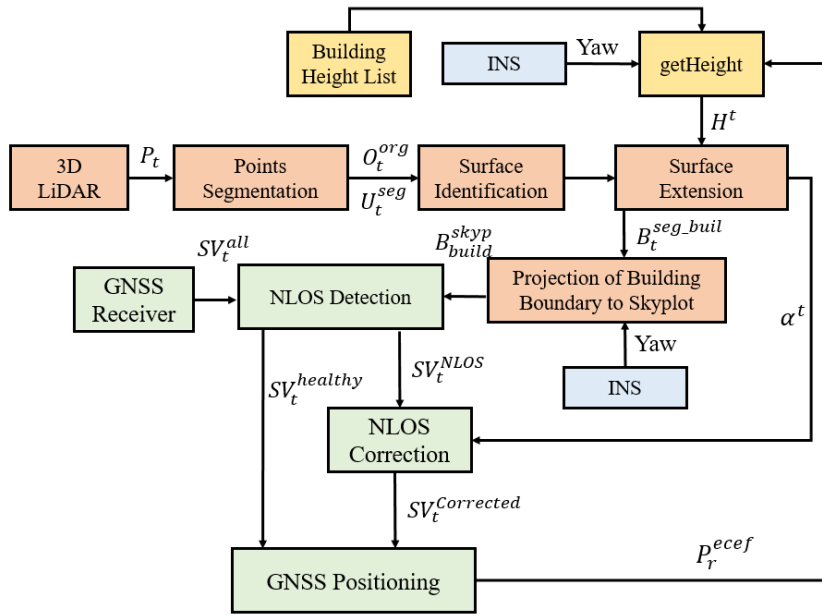
Fig.2 Illustration Overview of the proposed algorithm of NLOS correction and corresponding positioning flowchart. The main inputs are GNSS raw measurements and real time point clouds from 3D LiDAR. The auxiliary inputs are yaw angle from INS and building height from Google Maps.

3. BUILDING SURFACE DETECTION AND TRANSFORMATION

To detect the buildings boundaries and obtain the corresponding distances from GNS receiver to buildings, a point cloud segmentation method is employed to effectively implement the building surface detection in this section.

3.1 Building Surface Detection and Transformation

The surrounding environment is expressed as points set $P_t = \{p_1, p_2, \dots, p_n, t\}$ at a given time t, where $p_i = (x_i, y_i, z_i,)$ represents the point at a given time t in the LiDAR coordinate system. To distinguish the building surface from the unordered points set and determine the distance from GNSS receiver to the building surface, two steps are needed: the segmentation and building surface identification. The segmentation process is summarized in detail as shown in Algorithm 1. Inputs of Algorithm

1 are points set and search radius r_{search}. Outputs include the bounding box [25] sets and organized point clusters, which indicate different objects around. The bounding box mentioned in Algorithm 1 is a function to get the bounding box that can represent the organized point cluster. Bounding box U_i is specifically determined by vector U_i as follows:

$$U_i = [x_i^c, y_i^c, z_i^c, roll_i^c, pitch_i^c, yaw_i^c, d_i^{len}, d_i^{wid}, d_i^{hei}] \tag{1}$$

Where x_i^c, y_i^c and z_i^c denote the position of the bonding box in x, y, and z directions respectively in LiDAR coordinate system. $roll_i^c, pitch_i^c$ and yaw_i^c denote the orientation of bounding box in LiDAR coordinate system. d_i^{len} is the length, d_i^{wid} is the width and d_i^{al} is the height of the bounding box.

Algorithm 1: Segmentation for points set $\boldsymbol{P_t}$

Input: points set $\boldsymbol{P_t} = \{\boldsymbol{p_1, p_2, …, p_n, t}\}$, search radius $\boldsymbol{r_{search}}$
Output: Bounding Box sets $\boldsymbol{U_t^{seg}} = \{\boldsymbol{U_1, U_2, …, U_i, … U_n, t}\}$,
Organized point clusters $\boldsymbol{O_t^{org}} = \{\boldsymbol{O_1, O_2, …, O_i, … O_n, t}\}$
1   create a Kd-tree representation for the input points set $\boldsymbol{P_t}$
2   setup an empty clusters list $\boldsymbol{C_t^{clt}}$ and an empty list to save
    points sets $\boldsymbol{P_t^{check}}$
3   **for all** points $\boldsymbol{p_i}$ in $\boldsymbol{P_t}$ **do**
4   add $\boldsymbol{p_i}$ to the points set $\boldsymbol{P_t^{check}}$
5   **for all** $\boldsymbol{p_i}$ in $\boldsymbol{P_t^{check}}$ **do**
6   search for the points set $\boldsymbol{N_i}$ of point neighbor of $\boldsymbol{p_i}$ in a
      sphere with radius r<$\boldsymbol{r_{search}}$
7   **for** every point $\boldsymbol{N_i^i}$ in points set $\boldsymbol{N_i}$ **do**
8   **if** $\boldsymbol{N_i^i}$ have not been processed
9   add $\boldsymbol{N_i^i}$ to points sets $\boldsymbol{P_t^{check}}$
10   **end if**
11   **end for** the points set $\boldsymbol{N_i}$
12   **if all** the points in $\boldsymbol{P_t^{check}}$ have been processed
13   add $\boldsymbol{P_t^{check}}$ to $\boldsymbol{O_t^{org}}$ as an organized points set
14   add $BoundingBox(\boldsymbol{P_t^{check}})$ to $\boldsymbol{U_t^{seg}}$ as a bounding box
15   reset $\boldsymbol{P_t^{check}}$ to empty
16   **end if**
17   **end for** $\boldsymbol{P_t^{check}}$
18 **end for** $\boldsymbol{P_t}$

To effectively identify the bounding box representing the surface building which can result in GNSS signal reflection and subsequent NLOS receptions, surface identification method is need and is summarized in detail as shown in Algorithm 2. The inputs of this algorithm are U_t^{seg} and O_t^{org} obtained from Algorithm 1, point number threshold num_{thres}, length threshold len_{thres} and height threshold hei_{thres}, building height list H_{build}, receiver position P_r^{ecef}, yaw angle Yaw_r from INS. The output is the bounding box set $B_t^{seg\_buil}$ specifically representing the building surface. The function Num mentioned in Algorithm 2 is used to count the points number of each cluster O_i. The function $getHeight$ is used to search the height information from a saved building height list which contains the height information. To determine the actual height of the identified building surface, P_r^{ecef}, U_i and Yaw_r are also needed. P_r^{ecef} indicates the GNSS position given by previous epoch positioning result. Relative position between GNSS receiver and detected building can be obtained from U_i. Moreover, the yaw angle Yaw_r can be acquired from INS. For each bounding box B_i, the distance α_i from receiver to the detected building surface can be calculated as follows:

$$\alpha_i = \sqrt{(x_i^{c2} + y_i^{c2} + z_i^{c2})} \tag{2}$$

Algorithm 2: Building surface identification from Bounding Box sets and height extension

---

Input: Bounding Box sets $U_t^{seg} = \{U_1, U_2, ..., U_i, ... U_n, t\}$, Organized point clusters $O_t^{org} = \{O_1, O_2, ..., O_i, ... O_n, t\}$, point number threshold num_{thres}, length threshold len_{thres} and height threshold hei_{thres}, building height list H_{build}, receiver position P_r^{ecef}, yaw angle Yaw_r from INS

Output: Bounding Box set represents building surfaces $B_t^{seg\_buil} = \{B_1, B_2, ..., B_i, ... B_n, t\}$

1 setup an empty clusters list $B_t^{seg\_buil}$ to save bounding box
2 **for all** bounding box U_i in U_t^{seg} do
3   if $Num(O_i) > num_{thres}$
4      $U_i \leftarrow [x_i^c, y_i^c, z_i^c, roll_i^c, pitch_i^c, yaw_i^c, d_i^{len}, d_i^{wid}, d_i^{hei}]$
5   if $d_i^{len} > len_{thres}$ and $d_i^{hei} > hei_{thres}$
6        $d_i^{hei} \leftarrow getHeight(H_{build}, P_r^{ecef}, U_i, Yaw_r)$
7        $B_i \leftarrow U_i$
8   **end if**
9   **end if**
10 **end for** U_t^{seg}

Thus, the bounding box with extended height representing the building surface can be identified with Algorithm 2. Height of the bounding box representing building surface can be extended to the real one. The bounding box is extended from rectangle ABCD to rectangle CDEF as can be seen in Fig. 3. Then, the boundary parameters for bounding box B_i corresponding to building surface are denoted by line segment $\overline{EF}$ denoted as B_{build}^{3d}, the matrix of bus boundary. To represent the bus, two points, E and F, are required. The B_{build}^{3d} is structured as follows:

$$B_{build}^{3d} = \begin{bmatrix} x_{3dE} & y_{3dE} & z_{3dE} \\ x_{3dF} & y_{3dF} & z_{3dF} \end{bmatrix} \tag{3}$$
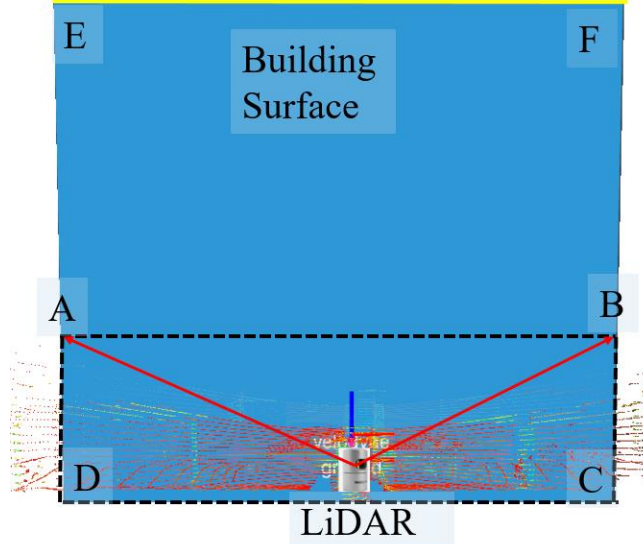
Fig.3 Illustration of point sets segmentation and building surface identification. Blue box ABCD represents the initially detected building surface. Blue box CDEF represents the extended building surface.
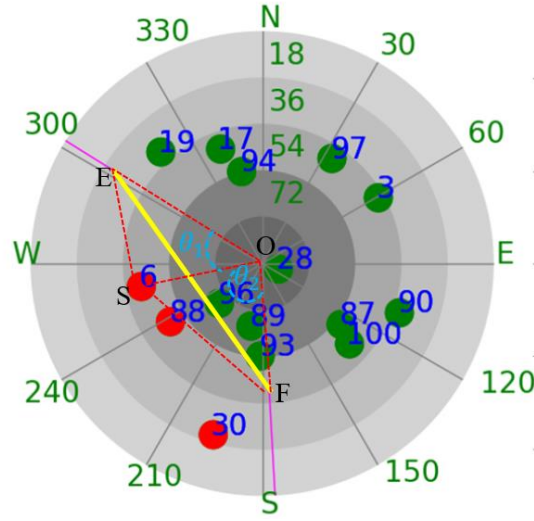
Fig.4 Skyplot of GNSS satellites and detected building surface boundary. Green and red circles and the nearby numbers indicates satellites and corresponding PRNs. Line segment $\overline{EF}$ indicates the boundary.

3.2 Coordinate Transform

To implement the algorithm of NLOS detection and subsequent correction, satellites' visibility need to be determined based on the extended boundaries of the detected building surfaces. Thus, the relative position of the GNSS receiver to satellites and to building surfaces need to be transformed into a same representation, the skyplot. In each epoch, information from satellites, including azimuth, elevation angles and SNR, can be obtained from the GNSS receiver. Part of satellite information can be represented as $SV_t^{all} = \{SV_1, SV_2, \ldots, SV_i, \ldots SV_n\}$. n represents the number of satellites received. SV_i represents the information for satellite i and $SV_i = \{az_i, el_i, SNR_i, \rho_i\}$. az_i denotes the satellite azimuth. el_i represents satellite elevation, SNR_i indicates satellite SNR and ρ_i denote the pseudorange measurement.

Satellite position can be easily indicated in the skyplot representation that is 2-dimension coordinate based on corresponding elevation and azimuth angles. A transformation matrix should be employed for building surface boundaries transformation from 3 dimensions coordinate to 2 dimensions coordinate. The transformation is conducted as the following formula.

$$B_{build}^{skyp} = B_{build}^{3d} G_T^{build} \tag{4}$$

where B_{build}^{3d} denotes the matrix of bus boundary presented in the previous sub-section. G_T^{build} is a 3x2 transform matrix. The B_{build}^{skyp} denotes the boundary matrix (2x2) in skyplot structured as follows:

$$B_{build}^{skyp} = \begin{bmatrix} x_{skyE} & y_{skyE} \\ x_{skyF} & y_{skyF} \end{bmatrix} \tag{5}$$

After the transformation, satellites and building surface boundary can be presented in the same coordinate, the skyplot, as shown in Fig. 4. Bounding box set $B_t^{seg\_buil} = \{B_1, B_2, \ldots, B_i, \ldots B_n, t\}$ can be transformed into $B_t^{skyp} = \{B_1^{skyp}, B_2^{skyp}, \ldots, B_i^{skyp}, \ldots B_n^{skyp}, t\}$, where B_i^{skyp} indicate the i_{th} boundary in the skyplot. Moreover, distance list representing the distance from GNSS receiver to the detected surface can also be obtained as $\alpha_t^{seg\_buil} = \{\alpha_1, \alpha_2, \ldots, \alpha_i, \ldots \alpha_n, t\}$, where α_i is associated with B_i^{skyp}. Line segment $\overline{EF}$ represents the building surface boundary corresponding to line segment $\overline{EF}$ as shown in Fig. 3. Then, the azimuth and the elevation angles for point E, and F can be calculated in the skyplot respectively.

4. IMPROVED GNSS POSITIONING WITH NLOS CORRECTION

In this section, NLOS error model is presented firstly. Then, NLOS detection criterion is proposed based on the detected building surface boundaries, satellite elevation angle, azimuth angle and SNR. NLOS error correction is implemented subsequently. Finally, GNSS positioning is conducted by WLS method using the healthy and corrected pseudorange measurements.

4.1 NLOS Correction Based on Building Boundary

In terms of the measurements from GNSS receiver, each pseudorange measurement ρ_n is written as follows [26].

$$\rho_n = R_n + c(\delta t^r - \delta t_n^{sv}) + I_n + T_n + \varepsilon_n \tag{6}$$

where R_n is the geometric range between the satellite and the GNSS receiver. δt_n^{sv} denotes the satellite clock bias. δt^r indicates the receiver clock bias. I_n represents the ionospheric delay distance; T_n indicates the tropospheric delay distance. ε_n represents the errors caused by the multipath effects, NLOS receptions, receiver noise, antenna delay, and so on. In this paper, we focus on mitigate the NLOS errors caused by environment buildings. In other words, shrinking ε_n by mitigate NLOS errors. The NLOS error model proposed in [9] is expressed in Fig. 5. The expected signal transmission route is expressed as dash blue line in Fig. 5. α represents the distance from receiver to the building. θ_{ele} represents the elevation angle of GNSS signal. Assuming the building is vertical to the ground and GNSS signal reflection satisfied the law of reflection. Thus, we can get $\theta_1 = \theta_2$. Moreover, the direction of real signal transmission is parallel to the direction of expected signal transmission. Finally, we have $\theta_1 = \theta_2 = \theta_0 = \theta_{ele}$. The route distance difference γ between the reflected signal and expected signal is indicated as follows:

$$\gamma = \gamma_1 + \gamma_2 \tag{7}$$

$$\gamma_1 = \alpha sec\theta_{ele} \tag{8}$$

$$\gamma_2 = \gamma_1 \cos(\theta_1 + \theta_2) \tag{9}$$

Thus, the NLOS error can be calculated with elevation angle and the distance from receiver to the building causing the reflection. In general, two steps are needed to proceed the NLOS correction. Firstly, NLOS detection is needed. Secondly, NLOS error calculation is needed.
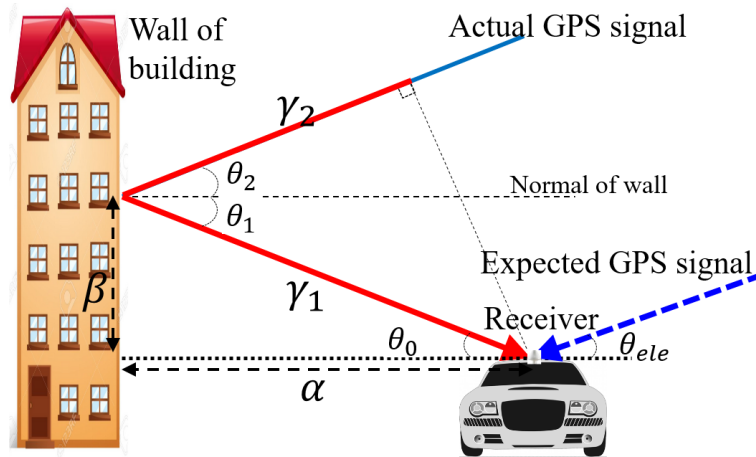
Fig.5 NLOS correction model. The signal is reflected by the building and received by receiver subsequently [9]

Algorithm 3: NLOS detection and correction

Input: Satellites information set $SV_t^{all} = \{SV_1, SV_2, \ldots, SV_i, \ldots SV_n\}$, bus boundary matrix $B_t^{skyp} = \{B_1^{skyp}, B_2^{skyp}, \ldots, B_i^{skyp}, \ldots B_n^{skyp}, t\}$, distance list $\alpha_t^{seg\_buil}$, area threshold $S_{threshold}$, SNR threshold $SNR_{threshold}$, threshold of boundary uncertainty θ_{thres}
Output: corrected satellites information set after NLOS identification: $SV_t^{cor} = \{SV_1^{cor}, SV_2^{cor}, \ldots, SV_i^{cor}, \ldots SV_m^{cor}\}$
1 **for all** boundary B_i^{skyp} in B_t^{skyp} do
2   **for all** satellites SV_i in SV_t^{all} do

3	estimate θ_1, θ_2 as shown in Fig. 4
4	Get triangle area $S_{\Delta SEO}$ of triangle SEO from B_i^{skyp}
5	Get triangle area $S_{\Delta SFO}$ of triangle SFO from B_i^{skyp}
6	Get triangle area $S_{\Delta SEF}$ of triangle SEF from B_i^{skyp}
7	Get triangle area $S_{\Delta EOF}$ of triangle EOF from B_i^{skyp}
8	$\Delta S = S_{\Delta SEO} + S_{\Delta SFO} + S_{\Delta SEF} - S_{\Delta EOF}$
9	**if** $(SNR_i > SNR_{threshold})$ or $(\theta_1 < \theta_{thres})$ or $(\theta_2 < \theta_{thres})$
10	**break**
11	**if** $\Delta S > S_{threshold}$ **and** $((\theta_1 + \theta_2) < \angle EOF < 180°$
12	**break**
13	**else**
14	$SV_i \leftarrow \{az_i, el_i, SNR_i, \rho_i\}$
15	$SV_i(\rho_i) \leftarrow SV_i(\rho_i) - (\gamma_1 + \gamma_2)$
16	$SV_i^{cor} \leftarrow SV_i$
17	**end if**
18	**end for** satellites set SV_t^{all}
19	**end for** boundary set B_t^{skyp}

The process of NLOS correction is summarized in detail in Algorithm 3. The inputs of the Algorithm 2 include satellites information SV_t^{all}, building surface boundaries information B_t^{skyp}, distance list $\alpha_t^{seg\_buil}$, area threshold $S_{threshold}$, SNR threshold $SNR_{threshold}$, threshold of boundary uncertainty θ_{thres}. The output is the corrected satellites information set SV_t^{cor}. Firstly, angle θ_1 and θ_2 shown in Fig. 4 are estimated. Then areas of triangle $S_{\Delta SEO}$, $S_{\Delta SFO}$, $S_{\Delta SEF}$ and $S_{\Delta EOF}$ are calculated and ΔS can be estimated subsequently. Secondly, GNSS measurement that SNR is larger than $SNR_{threshold}$ will not be excluded as signal with strong SNR may not be reflected by buildings. To avoid the faulty exclusion, a heuristically determined threshold $S_{threshold}$ is set. Satellites whose positions are quite near the extended edge beam ($\theta_1 < \theta_{thres}$ or $\theta_2 < \theta_{thres}$) also should not be excluded, such as the satellite 93 in Fig. 4, thus the angle threshold θ_{thres} is set. Satellites whose positions are quite near the building surface boundary should not be identified as NLOS which can be determined by comparing ΔS and $S_{threshold}$, such as the satellite 96 in Fig. 4. Finally, the pseudorange measurements from NLOS receptions can be corrected by the NLOS error model.

In this case, these NLOS satellites can be detected and corresponding pseudorange measurements are corrected.

4.2 GNSS Positioning Based on corrected Pseudorange Measurements

Measurements with low elevation and SNR are more likely to be a contaminated GNSS signals, such as the multipath or NLOS, due to the reflection, blockage and diffraction. Thus, proper thresholds need to be set to exclude the unhealthy measurements. For satellite SV_i, if ele_i is less than ele_{thres} or SNR_i is less than SNR_{thres}, it should be excluded from GNSS positioning. Pseudorange measurements in SV_t^{cor} will be employed for GNSS positioning calculation.

The clock bias between GNSS receiver and satellites is usually represented by the pseudorange measurements. The equation linking the receiver position and satellite can be structured as the following formula using least square (LS) method:

$$\hat{x} = (G^T G)^{-1} G^T \rho \tag{10}$$

where G represents the observation matrix and is structured by unit LOS vectors between GNSS receivers position and satellites position. $\hat{x}$ indicates the estimated receiver position and ρ denotes the pseudorange measurements.

To better represent the quality of each measurement based on the information measured by receiver, weightings of each satellite are needed. Function to calculate the weighting by integrating the measurement SNR and satellite elevation is expressed as [22]:

$$W^{(i)}(ele_i, SNR_i) = \begin{cases} \frac{1}{sin^2 ele_i}\left(10^{-\frac{(SNR_i-T)}{a}}\left(\left(\frac{A}{10^{-\frac{(F-T)}{a}}} - 1\right)\frac{(SNR_i-T)}{F-T} + 1\right)\right) & SNR_i < T \\ 1 & SNR_i > T \end{cases} \tag{11}$$

where $W^{(i)}(ele_i, SNR_i)$ denotes the weighting for satellite SV_i. The parameter T indicates the threshold of SNR and is equal to $SNR_{threshold}$. Parameter a, A and F in (8) are experimentally determined. Then, the weighting matrix W is a diagonal matrix constituted by $W^{(k)}(ele_i, SNR_i)$. Finally, GNSS receiver position can be estimated using WLS method as:

$$\hat{x} = (G^T W G)^{-1} G^T W \rho \tag{12}$$

Note that both LS (10) and WLS (12) positioning methods are compared in the experiment section.

5. EXPERIMENT EVALUATION

5.1 Experiment Setup

A dynamic experiment is conducted in urbanized area in Hong Kong with buildings on both sides, which can be seen in Fig. 6. The u-blox M8T receiver is used to collect raw GPS and BeiDou measurements. 3D LiDAR sensor, Velodyne 32, is employed to provide the real-time point clouds scanned from the surrounding buildings. Both u-blox receiver and 3D LiDAR are installed on the top of a vehicle during the experiment. The red curve in Fig. 6 indicates the driving path of vehicle. The data were collected within approximately 2 minutes' drive at a frequency of 1 Hz. The ground truth is generated by NovAtel SPAN-CPT. To verify the effectiveness of the proposed NLOS correction method, four positioning solutions are compared:

- LS positioning (LS)

- WLS positioning (WLS)

- WLS positioning + NLOS exclusion (WLS-NE)

- WLS positioning + NLOS correction (WLS-NC)

The third method excludes the NLOS satellites from GNSS positioning before WLS. In this experiment section, parameters mentioned above can be referrer in TABLE I.

5.2 Comparison of Different GNSS Positioning Solutions

The experiment results of GNSS positioning using the four methods are shown in TABLE 2. The LS method can achieve only 81.53 meters of mean errors and 114.38 meters of standard deviation among the dynamic test. Only 1.77% of the positioning result own an error which is less than 15 meters and 59.29% of the results possess an error more than 40 meter. Considerable improvements are introduced with the aid of weights for each satellite using WLS method. The mean positioning error and standard deviation are decreased to 42.15 meters and 21.29 meters respectively. This means that the presented weights make the positioning result more accurate and smooth. The percentage of errors which are less than 15 meters is increased to 8.04%. Moreover, only 27.68% of the positioning result containing an error which is less than 40 meters. However, after excluding the satellites that are blocked by the buildings using WLS-NE method, the positioning result is severely degraded with the positioning error going up to 394.05 meters and corresponding standard deviation increasing to 241.01 meters. Meanwhile, all the positioning results are larger than 30 meters and even 98.23% of the results possess an error which is more than 40 meters. This is because of the dramatic decrease in the number of satellites available for GNSS positioning. As we can see from Fig. 7, the red circles indicate the satellites that are blocked by buildings and the green satellites indicates the healthy satellites. After the exclusion of the blocked satellites, only 6 satellites are available for GNSS positioning and all of them possess high elevation angles which are all larger than 54 degrees. The can dramatically increase the value of horizontal dilution of precision (HDOP), which will consequently magnify the effects of pseudorange measurements errors in the GNSS positioning result. In overall, the WLS method obtains best performance among the three GNSS positioning methods.

Distinct improvements are obtained using the proposed method, comparing with the WLS method. Firstly, the mean positioning error is decreased from 42.15 meters to 26.7 meters and 36.67% of improvement is obtained. This significant improvement is obtained due to the proposed NLOS corrections and means that the satellites with low elevation are actually blocked and then reflected by surrounding buildings. Interestingly, the standard deviation is slightly increased from 21.29 meters to 24.32 meters. Secondly, the percentage of positioning errors which are less than 15 meters is increased dramatically from 8.04% to 56.25%. Moreover, 82.14% of the positioning results possess an error less than 30 meter. Finally, only 13.39% of the positioning results own an error that is more than 40 meters. In overall, evident improvements are obtained with the proposed NLOS correction method. Comparing to the WLS-NE method, the proposed method utilizes the NLOS receptions and correct the corresponding NLOS measurements, the HDOP will not increase and better satellites geometry distribution is obtained.

The detailed positioning results is shown in Fig. 8. The top panel indicates the surface detection with the red line representing the ground truth and blue line denoting the proposed detection results. Approximately 98% of detection accuracy is obtained

during the dynamic test. The middle panel indicates the satellites numbers available for GNSS positioning. In some epochs, the number of satellites available is quite small. The button panel indicates the positioning results using WLS and WLS-NC methods.

Fig.6 Environemnt that the data were collected on a urbanized road with both side filled with buildings.
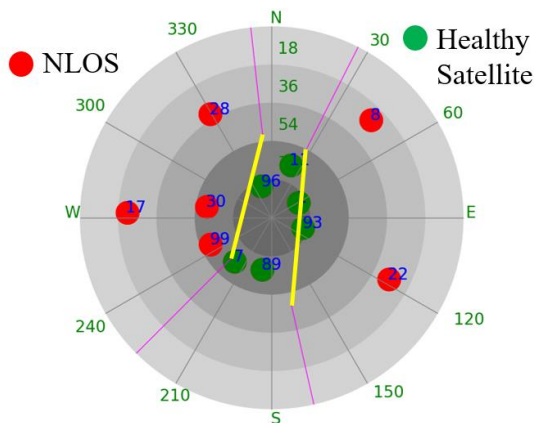
Fig.7 Skyplot indicating the satellites distribution during the dynamic experiment. Green circle represents the satellites that are healthy. Red circle denotes the NLOS satellites. Yellow line indicates the building surface boundary.
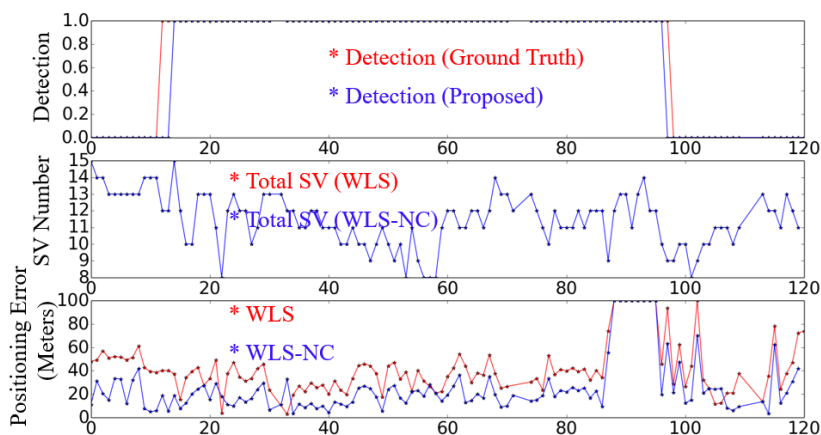
Fig.8 Experimental results of WLS-ESF and WLS-ESF-NE, which depicted in red and blue dots, respectively. Top panel indicates the building surface detection result.Middle panel inciates the numbers of satellites used. Button panel indicates the 3D positioning errors.

TABLE.1 PARAMETER VALUES USED IN THIS PAPER

Parameters	$S_{threshold}$	$SNR_{threshold}$	ele_{thres}	θ_{thres}
Value	10	45 dB-Hz	20°	5°
Parameters	a	A	F	
Value	30	32	10	

TABLE.2 POSITIONING PERFORMANCE OF THE FOUR METHODS (IN THE UNIT OF METER)

All data	LS	WLS	WLS-NE	WLS-NC
Mean error	81.53	42.15	394.05	26.7
Std	114.38	21.29	241.01	24.32
Percentage (<15 meters)	1.77%	8.04%	0%	56.25%
Percentage (<30 meters)	13.27%	41.96%	0%	82.14%
Percentage (>40 meters)	59.29%	27.68%	98.23%	13.39%

5.3 Performance Evaluation with Correcting NLOS Delay from Different Elevation Angles

Only certain satellites whose elevation angles are between certain elevation angles ranges will be corrected in each test. The objective is to analysis the percentages of NLOS errors introduced by each range of satellites. TABLE 3 shows the results of three separated NLOS correction tests. Firstly, if the satellites 8, 17, 22 and 28, whose elevation angles are between 18°~36°, are corrected with the proposed method, the mean positioning error is decreased from 42.15 meters to 29.93 meters comparing with the WLS method. 12.22 meters of improvement is obtained. Interestingly, the corresponding standard deviation also increase slightly. Approximately 79.64% of the positioning results own an error which is less than 30 meters. Secondly, only one satellite, satellite 88, possess an elevation angle which is between 36°~54° and is NLOS. Slight improvement is introduced after the correction with a mean positioning error of 41.95 meters and standard deviation of 21.80 meters respectively. 0.2 meters of improvement is obtained. Moreover, the percentage of positioning results which is more than 40 meters is similar to the results from WLS. Thirdly, two satellites, satellites 30 and 99 own an elevation which is between 54°~72°. Slight improvement (0.14 meters) is obtained with the proposed NLS corrections. The corresponding percentages is similar to the result from NLOS correction of elevation range (36°~54°). In summary, the NLOS satellites with lower elevation (18°~36°) introduce larger positioning errors, comparing with the NLOS satellites with higher elevation (36°~72°) and this is concurrent with the NLOS error model.

TABLE.3 POSITIONING PERFORMANCE OF WLS-NC WITH MANUAL SATELLITE SELECTION (IN THE UNIT OF METER)

All data	Elevation (18°~36°)	Elevation (36°~54°)	Elevation (54°~72°)
Mean error	29.93	41.95	42.01
Std	24.62	21.80	21.81
Percentage (<15 meters)	51.32%	7.96%	8.03%
Percentage (<30 meters)	79.64%	43.36%	39.29%
Percentage (>40 meters)	15.04%	28.32%	30.36%
Improvement	12.22	0.2	0.14
Satellites PRN	8,17,22,28	88	30,99

6. CONCLUSIONS AND FUTURE WORK

With the increasing attention in autonomous driving, GNSS owns increasing positioning requirement in accuracy and robustness. As mentioned in [8], NLOS is the dominant source resulting in unsatisfactory GNSS positioning result in super-urbanized area. NLOS exclusion is a commonly studied idea to improve GNSS positioning and some improvements can be obtained in some sub-urban scenarios. From the result presented in section V-B, However, as we can see from TABLE 2, NLOS exclusion can result in dramatically larger positioning errors (394.05 meters) and standard deviations (241.01 meters) in super urbanized area. NLOS correction is needed to radically mitigate the NLOS errors.

To mitigate the NLOS errors without ray-tracing process, this paper proposed a novel method to detect and correct the NLOS receptions. This study firstly employs the 3D LiDAR to detect the building surface and then integrate the building height information to extend the detected building to the actual height. Then, the NLOS detection and correction algorithm is proposed to correct the unhealthy pseudorange measurements from NLOS receptions. Thirdly, GNSS positioning is conducted using the healthy and corrected pseudorange measurements. According to the experiment results, the proposed method can correct the NLOS receptions and an improved GNSS positioning is obtained. From the result presented in section 5.3, majority of NLOS errors are caused by low elevation angle (18°~36°). Moreover, the satellite blocked by buildings with lower elevation angle is more likely to be reflected by the other buildings, thus causing the NLOS receptions.

In the near future, GNSS/LiDAR integration with NLOS corrections will be studied and corresponding dynamic experiment will be implemented in super-urbanized area with complicated traffic conditions to evaluate the effectiveness of the proposed method.

REFERENCES

[1]   Y. Gao, S. Liu, M. M. Atia, and A. Noureldin, "INS/GPS/LiDAR integrated navigation system for urban and indoor environments using hybrid scan matching algorithm," *Sensors,* vol. 15, no. 9, pp. 23286-23302, 2015.

[2]   Y. Gu, L.-T. Hsu, and S. Kamijo, "GNSS/Onboard inertial sensor integration with the aid of 3-d building map for lane-level vehicle self-localization in urban canyon," *IEEE Transactions on Vehicular Technology,* vol. 65, no. 6, pp. 4274-4287, 2016.

[3]   J. Levinson and S. Thrun, "Robust vehicle localization in urban environments using probabilistic maps," in *Robotics and Automation (ICRA), 2010 IEEE International Conference on*, 2010, pp. 4372-4378: IEEE.

[4]   X. Meng, H. Wang, and B. Liu, "A Robust Vehicle Localization Approach Based on GNSS/IMU/DMI/LiDAR Sensor Fusion for Autonomous Vehicles," *Sensors,* vol. 17, no. 9, p. 2140, 2017.

[5]   A. Fernández *et al.*, "ATENEA: Advanced techniques for deeply integrated GNSS/INS/LiDAR navigation," in *Satellite Navigation Technologies and European Workshop on GNSS Signals and Signal Processing (NAVITEC), 2010 5th ESA Workshop on*, 2010, pp. 1-8: IEEE.

[6]   A. Fernández, P. Silva, and I. Colomina, "Real-time navigation and mapping with mobile mapping systems using LiDAR/Camera/INS/GNSS advanced hybridization algorithms: description and test results," in *Proceedings of the 27th International Technical Meeting of the Satellite Division of the Institute of Navigation, ION GNSS 2014*, 2014, pp. 896-903.

[7]   L.-T. Hsu, H. Tokura, N. Kubo, Y. Gu, and S. Kamijo, "Multiple faulty GNSS measurement exclusion based on consistency check in urban canyons," *IEEE Sensors Journal,* vol. 17, no. 6, pp. 1909-1917, 2017.

[8]   J. Breßler, P. Reisdorf, M. Obst, and G. Wanielik, "GNSS positioning in non-line-of-sight context—A survey," in *Intelligent Transportation Systems (ITSC), 2016 IEEE 19th International Conference on*, 2016, pp. 1147-1154: IEEE.

[9]   L.-T. Hsu, "Analysis and modeling GPS NLOS effect in highly urbanized area," *GPS solutions,* vol. 22, no. 1, p. 7, 2018.

[10]   S. H. Kong, "Statistical Analysis of Urban GPS Multipaths and Pseudo-Range Measurement Errors," *IEEE Transactions on Aerospace & Electronic Systems,* vol. 47, no. 2, pp. 1101-1113, 2011.

[11]   D. Maier and A. Kleiner, "Improved GPS sensor model for mobile robots in urban terrain," in *Robotics and Automation (ICRA), 2010 IEEE International Conference on*, 2010, pp. 4385-4390: IEEE.

[12]   C. Pinana-Diaz, R. Toledo-Moreo, D. Betaille, and A. F. Gomez-Skarmeta, "GPS multipath detection and exclusion with elevation-enhanced maps," in *Intelligent transportation systems (ITSC), 2011 14th International IEEE Conference on*, 2011, pp. 19-24: IEEE.

[13]   S. Peyraud *et al.*, "About Non-Line-Of-Sight Satellite Detection and Exclusion in a 3D Map-Aided Localization Algorithm," *Sensors,* vol. 13, no. 1, pp. 829-847, 2013.

[14]   L.-T. Hsu, Y. Gu, and S. Kamijo, "3D building model-based pedestrian positioning method using GPS/GLONASS/QZSS and its reliability calculation," (in English), *GPS Solutions,* vol. 20, no. 3, pp. 413–428, 2016.

[15]   S. Miura, L.-T. Hsu, F. Chen, and S. Kamijo, "GPS error correction with pseudorange evaluation using three-dimensional maps," *IEEE Transactions on Intelligent Transportation Systems,* vol. 16, no. 6, pp. 3104-3115, 2015.

[16]   M. Obst, S. Bauer, P. Reisdorf, and G. Wanielik, "Multipath detection with 3D digital maps for robust multi-constellation GNSS/INS vehicle localization in urban areas," in *Intelligent Vehicles Symposium (IV), 2012 IEEE*, 2012, pp. 184-190: IEEE.

[17]   T. Suzuki and N. Kubo, "Correcting GNSS multipath errors using a 3D surface model and particle filter," *Proc. ION GNSS+ 2013,* 2013.

[18]   Y.-W. Lee, Y.-C. Suh, and R. Shibasaki, "A simulation system for GNSS multipath mitigation using spatial statistical methods," *Computers & Geosciences,* vol. 34, no. 11, pp. 1597-1609, 2008.

[19]   K. Ali, X. Chen, F. Dovis, D. De Castro, and A. J. Fernández, "GNSS signal multipath error characterization in urban environments using LiDAR data aiding," in *Satellite Telecommunications (ESTEL), 2012 IEEE First AESS European Conference on*, 2012, pp. 1-5: IEEE.

[20]   X. Chen, F. Dovis, M. Pini, and P. Mulassano, "Turbo architecture for multipath mitigation in global navigation satellite system receivers," *IET Radar, Sonar & Navigation,* vol. 5, no. 5, pp. 517-527, 2011.

[21]   J. I. Meguro, T. Murata, J. I. Takiguchi, Y. Amano, and T. Hashizume, "GPS multipath mitigation for urban area using omnidirectional infrared camera," *IEEE Transactions on Intelligent Transportation Systems,* vol. 10, no. 1, pp. 22-30, 2009.

[22]   T. Suzuki, M. Kitamura, Y. Amano, and T. Hashizume, "High-accuracy GPS and GLONASS positioning by multipath mitigation using omnidirectional infrared camera," in *IEEE International Conference on Robotics and Automation*, 2011, pp. 311-316.

[23]   J. Levinson *et al.*, "Towards fully autonomous driving: Systems and algorithms," in *Intelligent Vehicles Symposium (IV), 2011 IEEE*, 2011, pp. 163-168: IEEE.

[24]   J. Wei, J. M. Snider, J. Kim, J. M. Dolan, R. Rajkumar, and B. Litkouhi, "Towards a viable autonomous driving research platform," in *Intelligent Vehicles Symposium (IV), 2013 IEEE*, 2013, pp. 763-770: IEEE.

[25]   G. Barequet and S. Har-Peled, "Efficiently approximating the minimum-volume bounding box of a point set in three dimensions," *Journal of Algorithms,* vol. 38, no. 1, pp. 91-109, 2001.

[26]   E. Kaplan and C. Hegarty, *Understanding GPS: principles and applications*. Artech house, 2005.